NUMERICAL SIMULATION OF VOLCANOGENIC TSUNAMI WAVE INUNDATION IN TONGA

Gede Pringgana[1], Lee S. Cunningham[2], Benedict D. Rogers[3]

Tsunamis, often linked to seismic events such as earthquakes, can also be triggered by volcanic eruptions, posing significant risks to coastal regions. This paper investigates the tsunami generated by the volcanic eruption in the Tonga Islands on January 15, 2022, focusing on the behaviour of overtopping tsunami waves and their interaction with coastal structures. The study utilizes video footage and data from social media, supplemented by location information from Google Maps, to establish the affected coastal area's characteristics. Accurate data on the shape and dimensions of nearby barriers was crucial for effective numerical modelling, which was carried out using DualSPHysics software. The numerical modelling results provide insights into offshore water surface elevation, wave velocity, bore impact forces, and pressure distribution on vertical barriers. These findings offer a preliminary approach to understanding the interaction between volcanic-induced tsunamis and coastal infrastructure, contributing to the development of effective mitigation strategies for enhancing community resilience to such events.

Keywords: volcanic-induced tsunami; numerical modelling; coastal structures; DualSPHysics

INTRODUCTION

Volcanogenic tsunamis

Tsunamis are devastating natural disasters that can heavily damage coastal regions, and whilst commonly associated with seismic events such as earthquakes, volcanic eruptions can also trigger tsunami waves. Volcanic activity can directly trigger the displacement of large volumes of water and submarine landslides caused by unstable volcanic flanks, leading to the formation of significant tsunami waves. Historical records indicate that around 8% of all tsunamis are the result of submarine volcanic eruptions (Mokhtari, 2016).

The geological and tectonic setting of certain regions can amplify the risk of volcano-induced tsunamis. For instance, the eruption of the Anak Krakatau volcano in Indonesia's Sunda Strait triggered a devastating tsunami that caused widespread destruction and loss of life along the associated coastlines. The 22 December 2018 tsunami from the flank collapse of Anak Krakatau volcano swept onto the coastlines of southeastern Sumatra and western Java without warning from earthquake induced ground shaking, highlighting the unpredictable and potentially deadly nature of these phenomena (Nagai et al. 2020). The eruption of the Hunga Tonga-Hunga Ha'apai submarine volcano in the South Pacific in January 2022 provided another example of the destructive power of volcano-triggered tsunamis (Borrero et al. 2023). The interaction of the erupting magma with the surrounding ocean generated a series of tsunami waves that wreaked significant damage on the nearby island of Tonga. The tsunami waves also travelled across the Pacific Ocean, causing damage as far away as the west coast of the United States and South America (Vömel et al. 2022).

Effective preparedness and risk management strategies are crucial in mitigating the impacts of volcano-induced tsunamis. Improving scientific understanding of the complex mechanisms underlying these events, through continued research and data collection, can inform the development of more accurate risk assessment models, thereby enhancing the chances of survival for those living in high-risk coastal areas. In addition, the implementation of structural and non-structural mitigation measures, such as the construction of tsunami-resistant infrastructure and the development of comprehensive emergency response plans, can further enhance community resilience in the face of these devastating natural disasters (Necmioğlu et al. 2023; Liu et al. 2020).

Determining the Unspecified Location of the Tsunami Event Based on Video Footage

Video footage of tsunami events holds valuable information, as it becomes an authentic source for various parties with different purposes. For example, governments use the information as a basis for policy-making related to emergency response during disasters, while communities use it to anticipate the wider potential impacts of the disaster. Additionally, video recordings during a disaster are useful for analyzing the event, which contributes to scientific development. For instance, when the tsunami hit Fukushima in 2011, a video recorded from a helicopter helped predict the velocity of tsunami wave propagation through visual observation (Yamashita et al. 2016). Another video recording taken during the 2004 tsunami event in Banda Aceh, Indonesia, helped researchers evaluate the forces of the tsunami acting on coastal structures, including bridges (Iemura et al. 2005), as well as assess sediment transport (Nandasena et al. 2011).

[1] Senior Lecturer, Civil Engineering Study Program, Faculty of Engineering, Udayana University.
[2] Reader in Structural Engineering, School of Engineering, The University of Manchester.
[3] Professor of Computational Hydrodynamics, School of Engineering, The University of Manchester.

Disaster videos are often recorded spontaneously with built-in smartphone cameras. Today, the widespread ownership of smartphones and rapid advancements in smartphone technology have revolutionized the way information is shared during disaster events. These devices have become invaluable tools for capturing and disseminating critical information in the aftermath of natural disasters, including tsunamis (Guinn et al. 2018; Madhavaram et al. 2017). However, amateur disaster videos often have minimal narration, capturing mainly images and natural sounds from the incident. They sometimes lack information about the precise location of the event. In fact, the location details of the disaster are crucial for post-disaster analysis, which requires specific information about the local situation. Therefore, determining the exact location where a video was recorded is essential, although finding this manually requires significant time and effort.

In this paper, the presence of a video recording of a tsunami event caused by a volcanic eruption in the Tonga Islands on January 15, 2022, sparked an interest in conducting a numerical study to understand the behaviour of overtopping tsunami waves and their interaction with coastal structures. The physical processes involved in the interaction of the tsunami with the coastal structures can be identified through visual observations from the video footage. The tsunami propagated as a series of waves, characterized by turbulent wave fronts advancing towards the shore. Upon reaching the coastal defence, the waves broke and subsequently overtopped onto the adjacent promenade. The overtopped water then propagated into the streets, impacting residential houses and continued to surge landward. Due to the relatively flat terrain, the return flow was not particularly noticeable; instead, the water appeared to accumulate on the land. Subsequent tsunami waves followed a similar pattern, repeating the observed processes.

This numerical study required comprehensive data surrounding the affected coastal areas, which cannot be obtained purely from the video. At the beginning of this investigation, while awaiting contact with the video's author, there was limited information surrounding the video recording. Therefore, the first step in this study was to determine the video's exact location. Once that was ascertained, the next steps were to determine the coastal bathymetry and geometry of the coastal defences, promenade and shore-side structures at that location in order to model boundary conditions as accurately as possible. The key steps used to determine the location of the video recording during the tsunami event are presented in the flowchart in Figure 1.

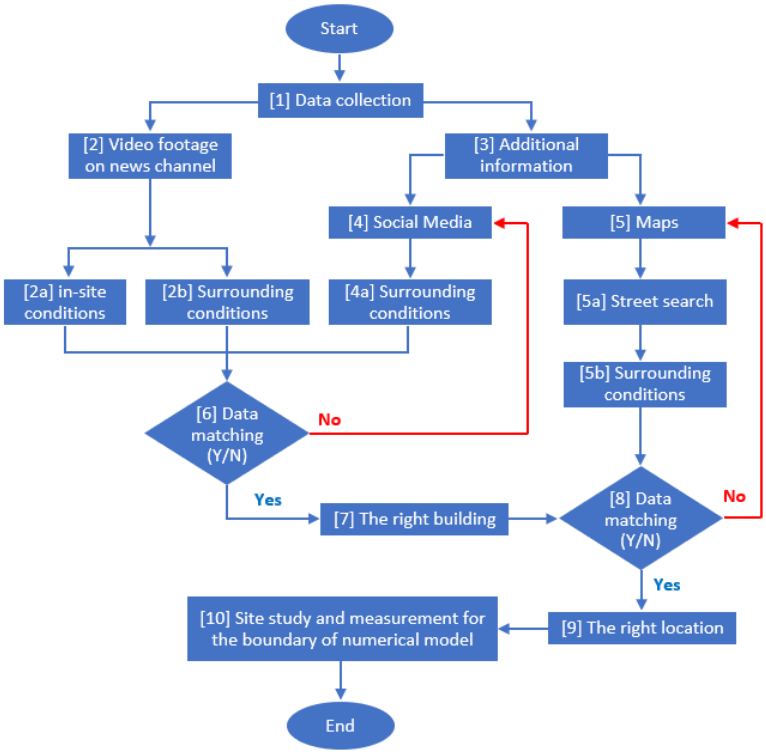

Figure 1. Steps to determine unspecified location of tsunami video recording.

In Figure 1, several steps are numbered in brackets […] to determine the unspecified location where the Tonga tsunami event occurred and which was subsequently broadcast worldwide via news channels

and social media. In Step [1], data collection is carried out, divided into Step [2] and Step [3], which correspond to available video footage and additional information as complementary sources, respectively. In Step [2], the initial video footage (Newsflare, 2022) shows several tsunami waves overtopping a low barrier on an unknown coastline in Tonga (Figures 2 and 3), without further details about its location. From the angle of the recording, it appears the video was shot from a certain height, likely from the roof of a building. In the video from Step [2], several details of the conditions were observed and divided into two parts. First, in Step [2a], the video reveals the situation near the recorder's position, such as a hipped-roof clad with corrugated sheeting. Second, in Step [2b], the conditions around the recorder were examined. In front of the recorder, there was a low coastal barrier, a road, trees, lined-up wooden stakes, and an electric pole (Figure 2). To the left of the recorder, there was empty land, a brick house fence, and a telecommunication tower in the distance (Figure 3). Similarly, undeveloped empty land was observed on the right side of the recorder. To obtain more information about the precise location of the targeted coastal area shown in the video footage, an inspection was conducted on tsunami-related photos and videos from Tonga through social media, as shown in Step [4].

Figure 2. Tsunami waves overtopping the coastal barrier (image used with permission, Newsflare (2022))

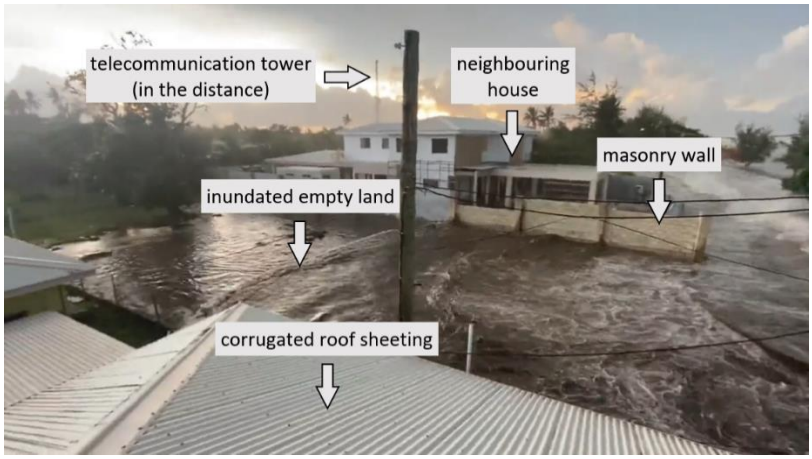

Figure 3. Tsunami waves inundating the area to the left of the video recorder (image used with permission, Newsflare (2022))

Among the many photos and videos of the 2022 Tonga tsunami event available online, a careful examination was conducted of their content, focusing on specific details in the surrounding area and in the distance, as outlined in Step [4a]. In Step [6], the information obtained from Steps [2a], [2b], and [4a] was compared until a video was found on the social media platform X (formerly Twitter) that contained details matching the information from those steps. Thus, in Step [7], it was concluded that the targeted coastal area shown in the video from Step [2] had been identified. The conditions around the coastal area are depicted in Figures 4, 5, and 6.

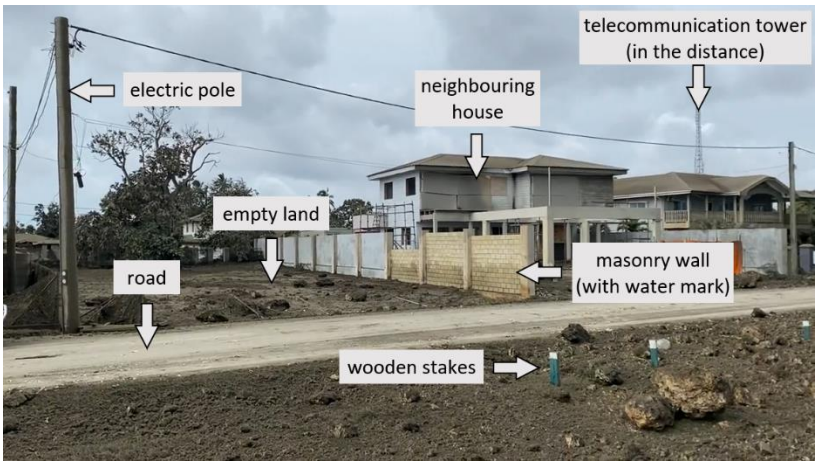

Figure 4. Neighbouring house after the tsunami with water marks on the fence's surface (image used with permission, Newsflare (2022))

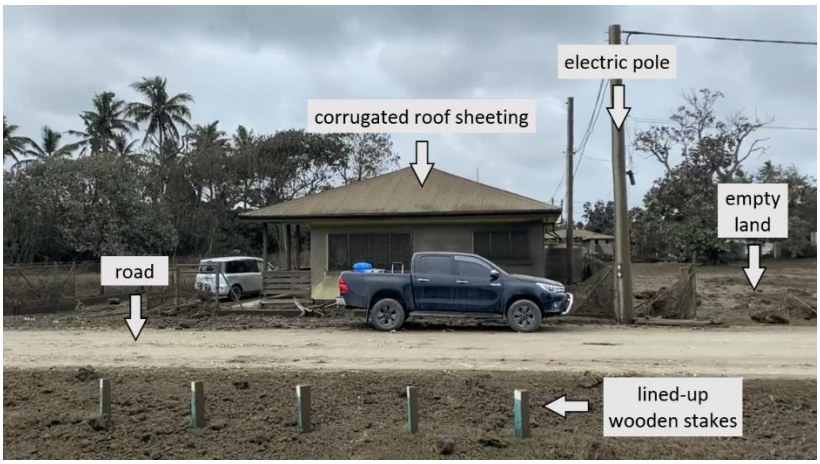

Figure 5. Post-tsunami condition of a house where tsunami video footage was recorded (image used with permission, Newsflare (2022))

Figure 6. Post-tsunami condition at the identified location in Nuku'alofa coastal area (image used with permission, Newsflare (2022))

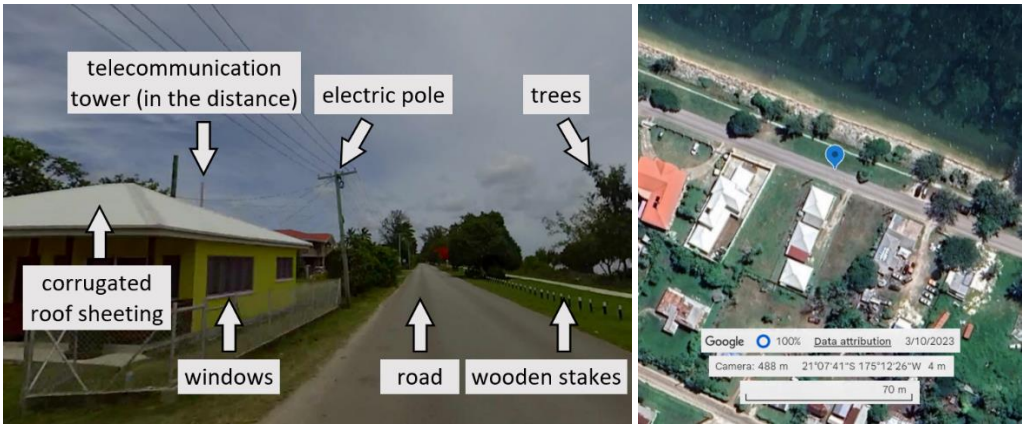

Figure 7. Google street (left) and satellite (right) views of the identified location in the Nuku'alofa coastal area (Google, 2024)

Furthermore, the coordinates of the targeted coastal area identified in Step [7] were examined using Google Maps [5]. In Step [5a], a search was conducted using Google Street View, focusing on residential buildings along near-shore streets. In Step [5b], each residential building was carefully examined, including specific details such as the shape of the roof and windows. In Step [8], the conditions around the houses were compared repeatedly until a location that matched the surrounding conditions of the targeted coastal area was found, as seen in Figure 7. To confirm this, the aerial view from Google Maps (Figures 7) was compared with the shape of the house roofs and surrounding conditions, matching those examined in Steps [2a], [2b], and [4a], as shown in Figures 2–6. Step [9] involves the confirmation of the location of the targeted coastal area. Finally, Step [10] involves conducting a site study and measurement using a topographic map.

NUMERICAL MODELLING

Numerical Modelling Set-up

In this study, numerical modelling of tsunami waves was carried out using the open-source smoothed particle hydrodynamics (SPH) software DualSPHysics version 5.2.2. The numerical modelling began with the design of a boundary model that replicates the conditions along the shoreline at Nuku'alofa, as seen in the video footage and shown in Figure 7. Details of the coastal area, including the shape and dimensions of the rubble mound coastal defence and roads, were obtained from the Coastal Resilience Project-Tonga report (GoT, 2017), and are redrawn in Figure 8. To be precise, the length of the road was determined using the scale available in Google Satellite View, as depicted in Figure 6.

Based on the available data, the boundary of the numerical model was designed with a total length, width, and height of 86 m, 5 m, and 7 m, respectively. The size of the numerical boundary was limited by the total number of SPH particles that could be run by the used GPU (NVIDIA GeForce RTX 3060). The size of the SPH particles was set to 0.025 m, with a total of 42,452,718 particles in the boundary of the numerical model. For a 35-second simulation (350 time-steps), the required runtime was 223 hours, approximately 9.3 days. Validation of the SPH model against experimental results, involving the SPH particle size and parameter values used in the DualSPHysics software, was carried out and is available in Cunningham et al. (2014) and Pringgana et al. (2016). Further studies demonstrating the efficacy and application of the SPH numerical method in relation to the orientations of coastal structures and barriers were presented in Pringgana et al. (2021) and Pringgana et al. (2023).

The numerical wave tank representing the focused location is shown in Figure 9 consists of onshore and offshore sections. For simplicity, the coastal defence has been modelled as non-porous. Further onshore, a 1.5m high wall represents the boundary walls of the residential properties evident from the video footage. In the offshore area, fluid particles representing seawater were pushed by a 7 m high piston-type paddle to generate solitary waves, simulating tsunami waves. The depth of still water and the distance of the paddle were set such that, within the simulation time, four solitary waves could be generated, propagating and overtopping the rubble mound barrier with sufficient water particles to inundate the onshore area, as observed with the repeatedly oncoming tsunami waves in the video footage. All solitary waves were generated based on Boussinesq wave theory (Goring, 1978), and measuring probes were set up to record water surface elevation, velocity, and pressure.

Based on video footage observation, the tsunami waves approached the shoreline as a wave train with random periods. Throughout the duration of the video, the clearest view occurred between the first and second oncoming tsunami waves, with an approximate period of 33 seconds. The periods of the later oncoming waves were more difficult to determine precisely, as they consisted of many smaller waves resembling wind waves. Among these smaller waves, the most significant one occurred approximately 23 seconds after the previous wave. Since the range of wave periods was wide, it is challenging to use this information with confidence.

On the other hand, another parameter that can be used as a reference for numerical modelling is the onshore tsunami bore velocity. Following the overtopping of the rubble mound, the velocities of the onshore tsunami bores were estimated to be around 5 m/s, based on the observation of the first two waves in the video. Although the first tsunami bore ran on wet land and the second on flooded land, their velocities were comparable. Thus, since the onshore tsunami bore velocity provided more reliable data than the oncoming wave period, it was used as a benchmark for determining the numerical wave profiles, include the still water level and the solitary wave height.

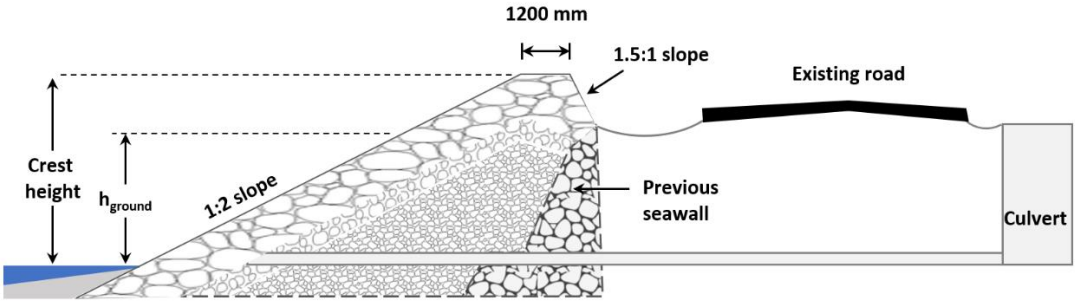

Figure 8. Typical section of rubble mound coastal defence at Nuku'alofa (adapted from GoT, 2017).

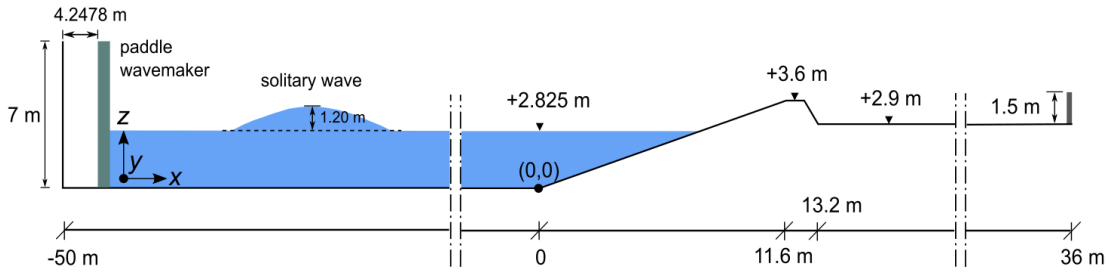

Figure 9. Schematic view of numerical water tank (not to scale).

Numerical Modelling Results

The solitary waves' propagation along the numerical water tank is shown in Figure 10. Figure 11 presents the offshore water surface elevation (WSE) measured at a distance of 5 meters seaward of the toe of the rubble mound. The first three offshore WSEs show stable solitary wave characteristics during their propagation and also indicate that the paddle distance was sufficient to maintain the initial water level, which helped create multiple solitary waves. However, the peak value of the fourth offshore WSE is about 19% higher than the others. An increase in the mean water level is expected due to a wave-setup-like phenomenon. However, this increase is caused by the accumulation of water particles between the oncoming fourth wave and the reflected third wave as it slopes over the rubble mound. The WSE of the fourth wave indicates that the paddle position had moved closer to the shoreline, which limited the number of solitary waves generated in this study.

The first and second solitary waves appear to have equal height, while the height of the third and fourth solitary waves tends to increase. Larger solitary waves were produced by a higher initial offshore water level as the paddle continued moving forward in the x-direction, while the paddle stroke (4.2478 m) and period (1 sec) remained constant for all solitary wave generations.

Figure 12 shows the offshore wave velocity measured at a location 5 meters seaward of the toe of the rubble mound, the same position as the WSE measurements. At this *x*-axis position, the plotted velocities were measured at three different heights: at the still water level, at half of the solitary wave

height, and at the top of the solitary wave height. Overall, each solitary wave has a different velocity history due to the dynamic movement of water particles around the sloping rubble mound. This dynamic is indicated by the negative velocity values as water particles move backward (in the negative *x*-direction).

Following wave overtopping, the solitary waves transitioned into a bore. Figure 13 illustrates the onshore bore velocity measured 20 meters landward of the toe of the rubble mound. The sharp increase in bore velocity is contributed by the rapid movement of the bore tip, followed by a larger amount of water particles. The negative velocity values indicate that some water particles bounced back after impacting the wall at the right end of the boundary model. Numerical predictions of onshore tsunami bore velocities were comparable to the tsunami bore velocities observed in the video footage.

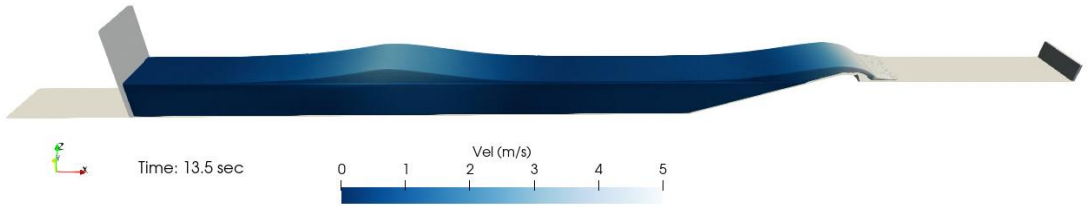

Figure 10. SPH numerical simulation of tsunami wave propagation.

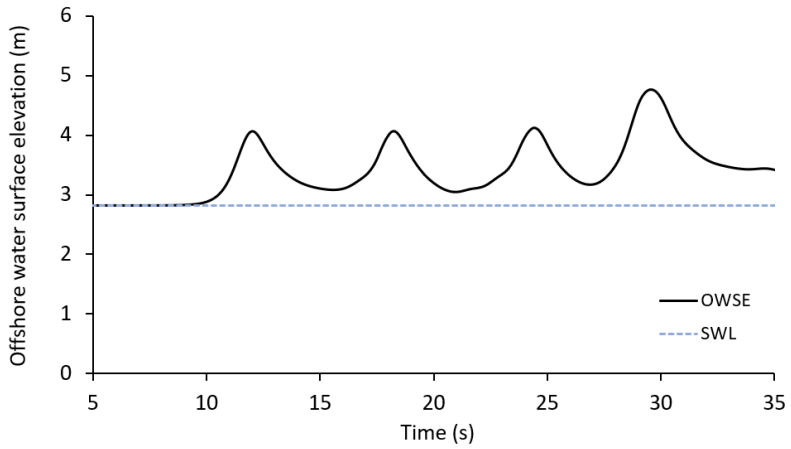

Figure 11. Offshore water surface elevation (WSE)

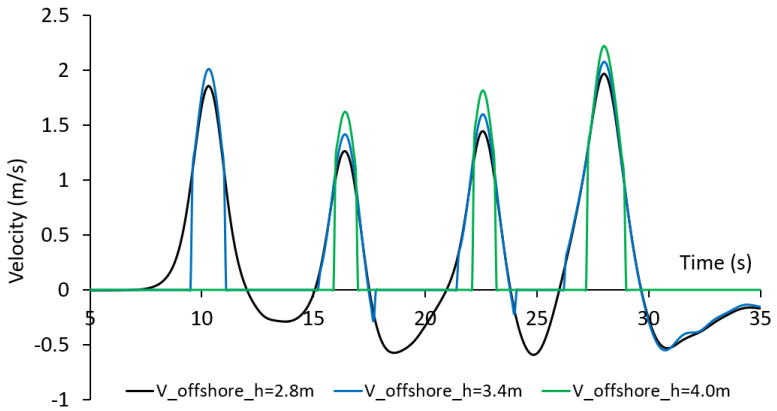

Figure 12. Offshore wave velocities

Figure 14 reveals the force-time history generated by the overtopped waves on the 1.5m high rear wall. The forces are significant in magnitude and could result in structural failure depending on the nature of the rear wall construction. Although damage was not reported in this location, damage to free-standing masonry walls was observed elsewhere in the event. In the numerical model, water overtopping the coastal defence was impounded by the rear landward wall with no gap for water particle outflow. As a result, once a water particle overtopped the rubble mound, it remained in the domain.

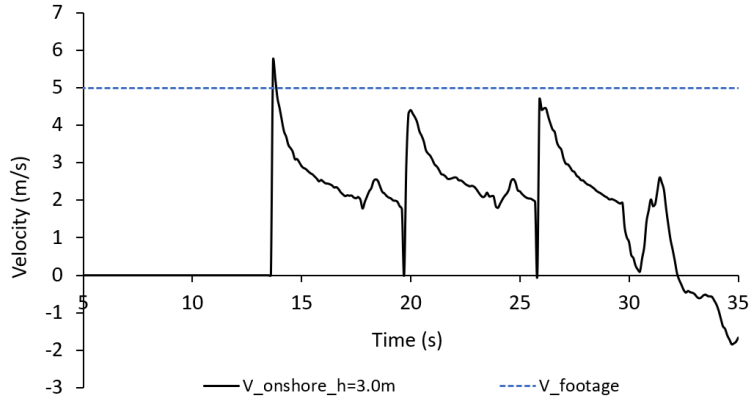

Figure 13. Onshore bore velocity

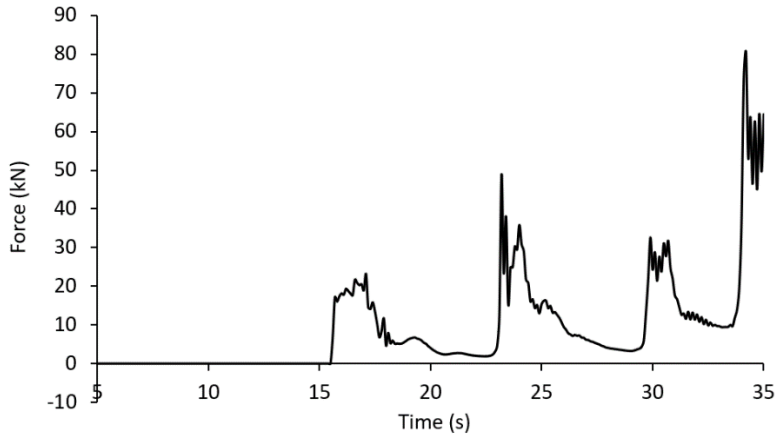

Figure 14. Impact force on vertical surface of the rear wall

The first bore impact was entirely caused by the leading tip of the bore (Figure 15), while the subsequent impacts were influenced by the oncoming leading bore interacting with the impounded water on the landward deck, as shown in Figure 16. This explains the irregularly increasing impact force depicted in Figure 14. The modelling also provided a bore pressure distribution as the bore hit the vertical wall, as illustrated in Figure 17, which is related to Figure 15. Figure 17 shows a random pattern of higher pressure, with the majority of the highest pressure occurring at the bottom part of the wall. Figure 17 was obtained by setting the wall to be transparent, with the view facing offshore.

The overall consistency between the numerical simulations and the tsunami video footage can be assessed by comparing the physical processes observable in the video, such as wave propagation, overtopping behaviour, and inundation patterns, with the simulated results. However, not all processes are directly comparable due to limitations in video coverage and duration, as well as the inherent simplifications and assumptions in the numerical model.

The numerical simulations correspond to the observations in the tsunami video footage to a certain degree. Offshore wave profiles were challenging to compare because the video focused exclusively on the very nearshore and onshore situation. Additional factors constraining the comparison include the wave type used to simulate the tsunami, the bathymetric representation, the wave generation mechanism, and the exclusion of certain physical phenomena, such as sediment transport and the presence of vegetation, which can influence flow dynamics. Among the observable parameters, the onshore bore

velocity was the closest match. Further investigation is necessary to assess the numerical hydrodynamic impact forces, which are considered moderate and have the potential to cause structural damage, Yeh et al (2014). As previously mentioned, the available video footage does not show any significant damage to coastal structures at the focused location. It is also not possible to ascertain the exact geometry and material properties of the impacted wall elements. Additional evidence may help provide clearer insights into the extent of any structural impacts.

Figure 15. Bore first impact on the wall, at *t* = 15.8 sec.

Figure 16. Interaction of second bore leading tip with impounded water, at *t* = 21 sec.

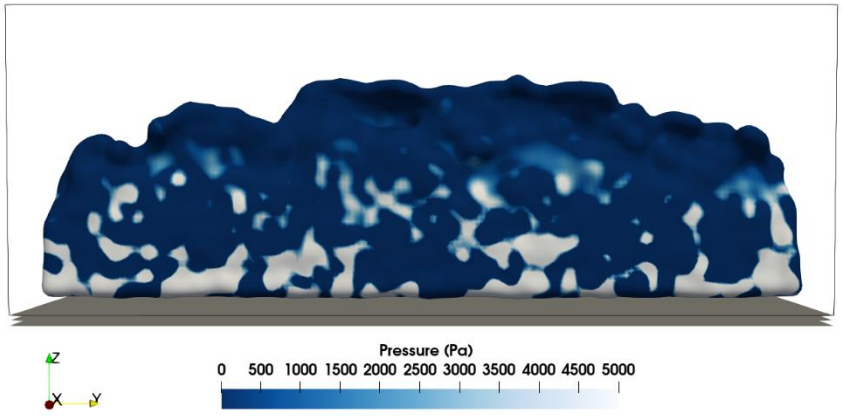

Figure 17. Tsunami bore pressure distribution on the wall's vertical surface, at *t* = 15.8 sec

CONCLUSION

This study highlights the significant impact that volcanic eruptions can have on tsunami generation, emphasizing the importance of understanding the interaction between tsunami waves and coastal structures. The investigation of the Tonga Islands tsunami on January 15, 2022, through video footage, social media data, and numerical modelling, provides valuable insights into wave behaviour, overtopping, and the effects on coastal infrastructure. The application of DualSPHysics software for numerical modelling, validated against experimental results, allowed for an in-depth analysis of wave velocity, impact forces, and pressure distribution on coastal structures. The results underscore the importance of accurate data in modelling tsunami events and offer a preliminary framework for understanding tsunami-structure interactions. These findings are critical for enhancing tsunami preparedness and resilience, supporting the development of more effective mitigation measures and infrastructure designs to better protect coastal communities from future volcanic-induced tsunamis.

Further research into the role of coastal structure orientation and barrier design is necessary to refine these models and improve disaster risk reduction strategies.

ACKNOWLEDGEMENTS

The authors would like to thank Dr. Faka'iloatonga Taumoefolau for granting permission to use his Tonga tsunami video footage, from which various stills have been reproduced as figures in this paper. The video footage was kindly provided via Newsflare, and we greatly appreciate their support in contributing to the quality of this work.

REFERENCES

Borrero, J.C., Cronin, S.J., Latu'ila, F.H. *et al.* 2023. Tsunami Runup and Inundation in Tonga from the January 2022 Eruption of Hunga Volcano. *Pure Appl. Geophys.* 180, 1–22.

Cunningham, L.S., Rogers, B.D., and G. Pringgana. 2014. Tsunami Wave and Structure Interaction: An Investigation with Smoothed-Particle Hydrodynamics. *Proceedings of the Institution of Civil Engineers: Engineering and Computational Mechanics*, 167(3), 126–138.

Google. 2024. Google Street View and Google Satellite image of Nuku'alofa coastal area [Street view image]. Google. https://www.google.com/maps/place/Nuku%CA%BBalofa,+Tonga., accessed 28/12/24.

Goring, D.G. 1978. Tsunamis – the Propagation of Long Waves onto a Shelf, W. M. Keck Laboratory of Hydraulic and Water Resources, California Institute of Technology, CA, USA, Report Kh-R-38.

Government of Tonga. 2017. Coastal Resilience Project – Tonga, Technical Feasibility Assessment (Annex II – Feasibility Study). Government of Tonga.

Guinn, V. L., Langhals, B., and J. Elshaw. 2018. Evaluating Smartphones for Infrastructure Work Order Management. *International Journal of Interactive Mobile Technologies (iJIM),* Kassel University Press, 12(8), 52-63.

Iemura, H., Pradono, M.H., and Y. Takahashi. 2005. Report on the Tsunami Damage of Bridges in Banda Aceh and Some Possible Countermeasures. *Proc. 28th JSCE Earthquake Engineering Symposium*, 1–10.

Liu, W., Li, L., Chen, L., Wen, M., Wang, J., Yuan, L., Liu, Y., and H. Li. 2020. Testing a Comprehensive Volcanic Risk Assessment of Tenerife by Volcanic Hazard Simulations and Social Vulnerability Analysis. *ISPRS International Journal of Geo-Information,* 9(273), 1-25.

Madhavaram, S., Matos, V., Blake, B., and R. Appan. 2017. ICTs in the context of disaster management, stakeholders, and implications. *Journal of Information Communication and Ethics in Society*, 15(1), 32-52.

Mokhtari, M. 2016. Introductory Chapter: A General Overview of Tsunami and Effectiveness of Early Warning System. *InTech*. doi:10.5772/65081.

Nagai, K., Arikawa, T., Pakoksung, K., Imamura, F., Watanabe, M., and H. Pan. 2020. Volcanic Eruption-Induced Tsunami at Anak Krakatau Volcano, Sunda Strait, Indonesia. *Proceedings of Conference on Coastal Engineering*, 36, currents.33.

Nandasena, N.A.K., Paris, R., and N. Tanaka. 2011. Numerical Assessment of Boulder Transport by the 2004 Indian Ocean Tsunami in Lhok Nga, West Banda Aceh (Sumatra, Indonesia). *Computers and Geosciences*, 37(9), 1391–1399.

Necmioğlu, Ö., Heidarzadeh, M., Vougioukalakis, G. E., and J. Selva. 2023. Landslide Induced Tsunami Hazard at Volcanoes: The Case of Santorini. *Pure and Applied Geophysics*, Birkhäuser, 180, 1811-1834.

Newsflare. 2022. *Watch moment Tonga is hit by tsunami after volcanic eruption* [Video]. Retrieved from https://www.newsflare.com/video/473708/tonga-tsunami, accessed 28/12/24.

Pringgana, G., Cunningham, L.S., and B.D. Rogers. 2016. Modelling of Tsunami-Induced Bore and Structure Interaction. *Proceedings of the Institution of Civil Engineers: Engineering and Computational Mechanics*, 169(3), 109–125.

Pringgana, G., Cunningham, L.S., and B.D. Rogers. 2021. Influence of Orientation and Arrangement of Structures on Tsunami Impact Forces: Numerical Investigation with Smoothed Particle Hydrodynamics. *Journal of Waterway, Port, Coastal, and Ocean Engineering*, 147(3): 04021006.

Pringgana, G., Cunningham, L.S., B.D. Rogers. 2023. Mitigating Tsunami Effects on Buildings via Novel Use of Discrete Onshore Protection Systems. *Coastal Engineering Journal*, 65(1), 149–173.

Vömel, H., Evan, S., and M.B. Tully. 2022. Water vapor injection into the stratosphere by Hunga Tonga-Hunga Ha'apai. *Science*, American Association for the Advancement of Science, 377(6613), 1444-1447.

Yamashita, K., Sugawara, D., Takahashi, T., Imamura, F., Saito, Y., Imato, Y., Kai, T., Uehara, H., Kato, T., Nakata, K., Saka, R., and A. Nishikawa, 2016. Numerical Simulations of Large-Scale Sediment Transport Caused by the 2011 Tohoku Earthquake Tsunami in Hirota Bay, Southern Sanriku Coast. *Coastal Engineering Journal*, 58(4), 1–28.

Yeh, H., Barbosa, A.R., Ko, H., and J. Cawley. 2014. Tsunami Loadings on Structures. *Coastal Engineering*, 1–13.